PHILOSOPHICAL TRANSACTIONS A

Phil. Trans. R. Soc. A.
doi:10.1098/not yet assigned

# Simulations of co-axial jet flows on Graphics Processing Units: the flow and noise analysis

**A.P. Markesteijn and S.A. Karabasov***

*School of Engineering and Material Science, Queen Mary University of London, Mile End Road, London, E1 4NS, UK / GPU-prime Ltd, Cambridge, UK*

**Keywords:** jet noise, large eddy simulation, acoustic analogy, similarity scaling, GPU computing, CABARET scheme

## Summary

Large Eddy Simulations (LES) are performed for a range of perfectly expanded co-axial jet cases corresponding to conditions of the Computation of Coaxial Jet Noise (CoJeN) experiment by QinetiQ. In all simulations, the high-resolution Compact Accurately Boundary-Adjusting high-REsolution Technique (CABARET) is used for solving the Navier-Stokes equations on unstructured meshes. The Ffowcs Williams – Hawkings method based on the penetrable integral surfaces is applied for far-field noise predictions. To correctly model the turbulent flow downstream of the complex nozzle that includes a central body, a Wall Modelled LES approach is implemented together with a turbulent inflow condition based on synthetic turbulence. All models are run on Graphics Processing Units (GPUs) to enable a considerable reduction of the flow solution time in comparison with the conventional LES. The flow and noise solutions are validated against the experimental data available with 1-2dB accuracy being reported for noise spectra predictions on the fine grid. To analyse the structure of effective noise sources of the jets, the covariance of turbulent fluctuating Reynolds stresses is computed and their characteristic scales are analysed in the context of the generalised acoustic analogy jet noise models. Motivated by self-similarity of single-stream axi-symmetric jet flows, a suitable non-dimensionalisation of the effective jet noise sources of the CoJeN jets is tested and its implications for low-order jet noise models are discussed.

## Introduction

Since Lighthill [1], most of the existing analytical, experimental, and computational studies have been devoted to noise generated by single-stream jet flows [2,3,4] including several NASA Small Hot Jet Acoustic Rig (SHJAR) experimental campaigns [5]. In comparison with single-stream jets, dual and multi-stream jet flows, which are typical of exhaust flows in modern turbofan aeroengines, are much less analysed. This can be attributed to the geometrical and physical complexity of the multi-stream jet flows, which are characterised by the interaction of multiple turbulent shear layers. Furthermore, in comparison with single-stream jets, co-axial jets correspond to a much larger parameter space that is more difficult to cover in the experiment or simulation. Up to present, only a few experimental campaigns have systematically studied the dual stream jet noise and provided public-domain databases of flow and noise data for validation of theoretical and computational models. One of these databases has been generated as the result of CoJeN: the EU-funded Computation of Coaxial Jet Noise project. The CoJeN database spans across a representative variation of high-speed bypass and core Mach numbers as well as the temperature ratios, which has been extensively studied experimentally using Particle Image Velocimetry (PIV) [6] and the near-field acoustic array technique [7], as well as a combination of PIV and Laser Doppler Anemometry (LDA) [8]. In addition to the experimental investigations, a variety of modelling approaches, ranging from Large Eddy Simulations (LES) to lower-fidelity modelling techniques, have been applied to analyse CoJeN noise generation and propagation mechanisms mainly as a validation exercise for computational codes. For example, the flow fields and the acoustic data from CoJeN are used in [9] for validation of

*Author for correspondence (s.karabasov@qmul.ac.uk).
†Present address: School of Engineering and Material Science, Queer Mary University of London, Mile End Road, London, E1 4NS

several Reynolds Averaged Navier Stokes (RANS) and Large Eddy Simulation (LES) methods. As an alternative to the expensive Navier-Stokes methods, a simpler and faster Lattice-Boltzmann Method (LBM) is used [10].

While the use of LES methods is becoming increasingly popular for high-fidelity jet noise modelling since, due to their unsteady nature, they capture a wide diversity of temporal scales typical of high-Reynolds number flows, their computational cost remains a stumbling factor in the simulation of complex jet flows, where the cost of high-fidelity modelling with Wall Modelled LES and hybrid RANS-LES schemes [11] is roughly comparable. The LES cost is linked to the high degree of simulation concurrency, which is challenging to achieve with a Navier-Stokes method on fully unstructured meshes to keep the simulation times affordable in comparison with simpler methods such as LBM. On the other hand, when used within an efficient parallel implementation with a small memory footprint to fully exploit advantages of modern computer architectures such as Graphics Processing Units (GPUs), the computational performance of Eulerian LES methods for high-fidelity jet noise modelling can be made comparable to the Lattice Boltzmann schemes without compromising the model fidelity.
In this article, an Eulerian LES method based on the CABARET method, which GPU implementation for single-stream jet flows was previously demonstrated in [12], is applied for dual-stream jet simulations corresponding to the CoJeN experiment. Originally, Compact Accurately Boundary-Adjusting high-REsolution Technique (CABARET) was introduced as a compact formulation of the second-order Upwind Leapfrog scheme [13,14,15]. In comparison with conventional $2^{nd}$-$3^{rd}$ order schemes, CABARET has superior dispersion and dissipation properties. Its computational stencil takes just one cell in space and time for advection equations in three dimensions. The stencil compactness is achieved by using separate conservation and flux variables which are staggered in space-time. For applications to rapidly varying flows including shock waves with non-uniform aerodynamic grids, CABARET has been generalised to a low-dissipative flux-corrected scheme based on the maximum principle [16]. Furthermore, the application of asynchronous time stepping allows one to time-march CABARET at a constant Courant number close to the optimal value (~0.5) for best accuracy of the scheme [17]. Importantly, all these upgrades are achieved while keeping the original compact explicit computational stencil to enable efficient parallel implementations with a minimal delay in transmitting the data between processes (minimal computing latency). In the framework of the Monotonically Integrated LES approach, CABARET is implemented to approximate the hyperbolic part of the 3D Navier-Stokes equations and applied to single-stream jet flow and noise modelling in combination with the permeable multiple-closing disk Ffowcs Williams – Hawking (FW-H) method [18]. In the current article, the GPU-CABARET method coupled with the FW-H scheme is applied for several CoJeN jet cases corresponding to a short-cowl nozzle geometry that includes a central body.
In comparison with the previous simulations based on the Monotonically Integrated LES framework which implied a laminar flow condition upstream of the nozzle exit, a Wall Modelled LES (WMLES) approach is implemented here following [19,20] for the first time in the CABARET literature. Another distinct novelty of the present work is application of an open-source synthetic turbulence generator developed by the University of Utah [21,22] to prescribe velocity fluctuations for a turbulent inflow boundary condition of the CABARET solution at the core and bypass inlets. Once validated, the LES solutions are used to investigate effective noise sources in the context of the Goldstein generalised acoustic analogy [22] and to examine common non-dimensionalisations of the acoustic source parameters for the CoJeN flows of interest in order to provide a useful reference for future co-axial jet noise prediction schemes.

# Methods

## A. Grid generation and turbulence modelling

Following [12], the GPU-CABARET models for CoJeN utilise the so-called split-hexa meshes. These meshes correspond to hanging node-type cells which are available in the semi-automatic mesh generation process using the OpenFOAM utility “snappyHexMesh” (sHM). This mesh utility enables hexa-dominant mesh generation from triangulated surface geometries (e.g. CAD geometry), an essential need for the LES treatment of complex geometries. Importantly, the sHM utility also has the capability to “snap” the mesh to the geometry as well as the ability to generate “layers” of body-fitted grid near the boundaries if need be. Importantly, thanks to the compactness of the CABARET stencil, its extension to non-uniform meshes of the sHM type is performed without a notable effect on the solution quality.
Fig.1 shows mesh elements in the 3D volume around the CoJeN nozzle geometry including zoom-in views of mesh details in the symmetry plane of the nozzle. In the framework of the OpenFOAM snappyHexMesh routine, for the wall modelling the size and thickness of the grid layers near the boundary can be precisely controlled, which involves adding body-fitted hexahedral layers near the viscous wall boundary. For example, during the automatic meshing procedure, the distance between the centre of the control volume closest to the boundary and the boundary itself can be kept within a certain distance. Using the suggested mesh generation technique, a good quality Cartesian mesh is obtained in the region of the jet shear layers whose density becomes coarser away from the central body. Profiles of the mesh density

distribution along the bypass nozzle lipline are shown in fig.2, where x=0 corresponds to the trailing edge of the central body of the nozzle. The profiles correspond to the two grids, Mesh #1 and Mesh #2 which are used in the current investigation. Their grid count is 82 $10^6$ and 50 $10^6$ control volumes, respectively. Mesh #2 is generated from Mesh #1 by uniformly decreasing the amount of cells in all directions, while the same snappyHexMesh logic is used regarding refinements and the boundary layer size to insure that both meshes correspond to the same resolution near the nozzle walls. SnappyHexMesh is instructed to generate a boundary layer with 3 cells per thickness of 0.0018Dj in the bypass nozzle diameter units with an expansion ratio of 2.0. In terms of the wall-normal units $y^+$, $y^+ = yu^*/\nu$, where $y$ is the wall-normal coordinate of the cell centre nearest to the wall, $u^*$ is the friction velocity estimated from the corresponding cell centre velocity, and $\nu$ is the kinematic viscosity, the grid resolution is estimated to be around 20-30 based on the Reynolds number (Re) of the flow in the experiment (based on the bypass nozzle diameter and velocity parameters, Re~3.0 $10^6$). Special attention is given to the shear layer development, where extra refinement regions are placed after the each lipline of the nozzles. The refinement location is determined from an initial run of the same flow conditions on the mesh without the refinement. Further, because of the expected wake after the central body, the mesh is kept dense after the nozzle exit. The final refined mesh is generated by the sHM routine using a script and takes several hours on 16 CPU cores without further user interaction.

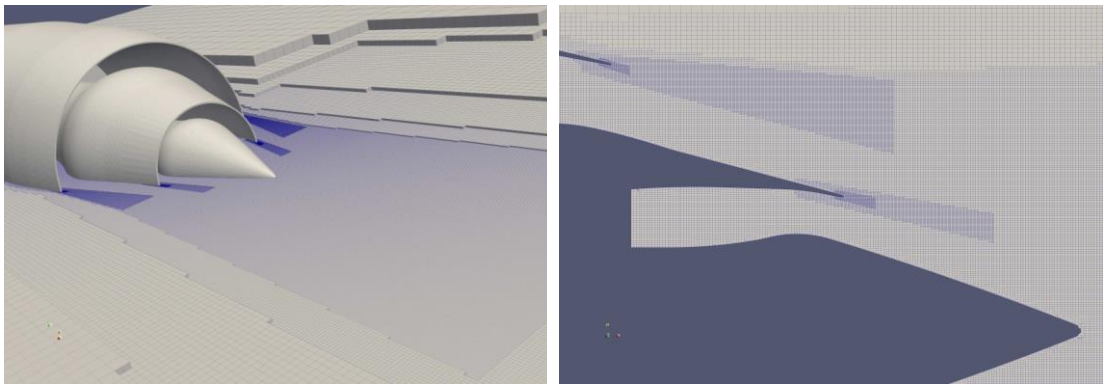

**Figure 1**. Overview of the sHM mesh for the CoJeN nozzle: a rendered 3D view (left) and mesh details in the symmetry plane (right).

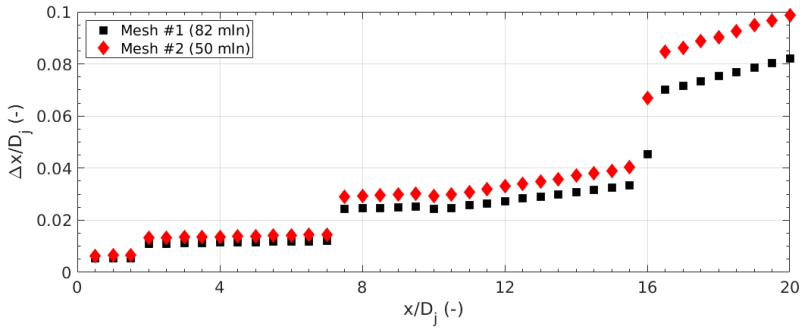


**Figure 2**. Mesh distribution along jet axis

Having generated a suitably refined grid around the nozzle geometry, following [19,20], the basic steps of the WMLES algorithm are implemented as follows. Inside the boundary layer mesh, each time step the cell centred values of the velocity and density are evaluated. These values are provided from CABARET to the wall model, which, in turn, returns the wall shear stress that is used as the wall boundary condition for CABARET. In particular, the wall model that has been employed in the present work is the one based on the algebraic method using Reichardt's law as described in [20]. Reichardt's law of the wall provides a relation between the dimensionless velocity in the boundary layer velocity units, $u^+ = U/\sqrt{\tau_w/\rho}$ and the dimensionless wall coordinate $y^+$. Here $\tau_w$ is the shear wall stress, $\rho$ is the local density, and $U$ is the local stream-wise velocity.

In accordance of the WMLES framework it is assumed the instantaneous velocity u can be used as an external boundary condition input for $u^+$. The resulting non-linear algebraic equation using u, y, and the laminar viscosity, is solved by a Newton iteration, giving the required wall shear stress. It should be pointed out that the computational cost of the wall model is negligible (less than 0.1%) in comparison with the overall LES cost.

In addition to the wall modelling, an open-source synthetic turbulence generator is applied to prescribe velocity fluctuations as a turbulent inlet flow boundary condition for each flow stream separately following [21,22]. This works by coupling a synthetic turbulence generator box of the same extent as the bypass and core inlet boundary face. Every time step the box velocity values are interpolated onto the boundary face coordinates. The fluctuations are added to the mean velocity part of the local Riemann invariants corresponding to the incoming waves of the one-dimensional characteristic boundary conditions, which are defined at each nozzle stream inlet based on the operational jet conditions [16,18,23]. There are two coupling parameters that control the amplitude and the timescale of the synthetic turbulence.
The use of the synthetic turbulence generator is motivated by the fact that although there are no data on turbulence measurements inside the CoJeN nozzles, boundary layers at the nozzle exit of a jet flow at the Reynolds number of the CoJeN jets are expected to be fully turbulent. Hence, in the absence of the experimental data and following the standard practice to prescribe inflow conditions in the jet LES literature [24], the amplitude parameter of the synthetic turbulence generator is chosen such that at the nozzle exit the average turbulent velocity fluctuations are around 3% of the stream-wise velocity. The time scale of the synthetic turbulence generator that scales with the stream-wise flow velocity inside the nozzle is adjusted accordingly so that the generated turbulent eddies are captured within several grid cells of the boundary layer, hence, allowing the CABARET solution to propagate a significant part of the synthetic turbulence from the inlets to the nozzle exit without strong dissipation. Before applying to the CoJeN nozzles, the parameters of the inflow synthetic turbulent conditions are verified on a flat plate flow test case.

B. Specification of the CoJeN cases

The main parameters of the 6 CoJeN cases considered in the present work are listed in table 1. All jets issue from the same axi-symmetric co-axial convergent nozzle geometry and exhaust in the atmosphere at normal pressure and temperature conditions, 99703 Pa and 288.14 K, respectively. Briefly, the 3 high-speed CoJeN cases, from OP1.1 to OP1.3, correspond to the same cold bypass velocity and the same heated core temperature but increasing the core stream velocity until it becomes transonic relative to the local sound speed in the heated core and supersonic in comparison with the ambient sound speed. The additional 3 jet cases (OP1.4, OP1.7 and OP1.8) correspond to a systematic change in the operational jet parameters in comparison with the fastest and, correspondingly, the nosiest OP1.3 jet flow. For example, parameters of the OP1.4 jet are obtained by simultaneously reducing velocities of the core and the bypass streams by, approximately, a factor of 1.4 while keeping the jet core temperature the same. The OP1.7 jet corresponds to an unheated version of OP1.4 where the bypass as well as the core Mach number remains approximately the same, consequently dropping the core velocity to the same level as the bypass. This also means OP1.7 is the single-stream equivalent of the dual-stream flow. Finally, for OP1.8 the velocity of the core stream is slightly increased, while keeping all parameters compared to OP1.7 the same.

**Table 1.** Operation Points of the CoJeN experiment

| **Operation Point:** | | **1.1** | **1.2** | **1.3** | **1.4** | **1.7** | **1.8** |
|---|---|---|---|---|---|---|---|
| **Core** | $U_j$ (m/s) | 340.3 | 404.5 | 480.7 | 341.5 | 218.4 | 241.7 |
| | $M_j$ | 0.621 | 0.738 | 0.877 | 0.620 | 0.642 | 0.712 |
| | $T_{sj}$ (K) | 775.6 | | | 785.0 | 287.8 | 287.0 |
| | $T_{tj}$ (K) | 827.9 | 849.5 | 879.9 | 837.2 | 311.5 | 316.0 |
| **Bypass** | $U_b$ (m/s) | 306.8 | | | 218.0 | 218.1 | 217.4 |
| | $M_b$ | 0.902 | | | 0.637 | 0.640 | 0.634 |
| | $T_{sb}$ (K) | 288.14 | | | 291.14 | 289.0 | 292.2 |
| | $T_{tb}$ (K) | 335.0 | | | 289.6 | 312.7 | 315.7 |

C. Far-field noise modelling

For all 6 Operation Points, the standard time-domain Ffowcs Williams –Hawkings (FW-H) method is used with permeable acoustic integration surfaces (details are in [3] and [18]). In the method, the LES solution is recorded on a set of integration surfaces, which enclose the jet turbulence and main vorticity regions in the jet shear layers, and then substituted in the semi-analytical free-space Green's function method to compute the far-field sound. The acoustic integration surfaces are of a funnel shape whose sides are parallel to the bypass shear layers (fig.3). The funnel surface is terminated with a sufficient number of the closing discs (~16) at the outlet to avoid pseudo-sound artefacts by averaging the noise spectra predictions produced by each individual disk. The resulting acoustic signal is computed for several polar angles to the jet flow corresponding to a geometrical far-field location. For converting the computed time signal to the far-field pressure power spectral density based on the common definition of 1Hz for the reference frequency and 20μPa

for the reference pressure, the standard statistical post-processing is applied based on the Welch method to deal with the Fourier Transform of short time series. Details of the LES signal post-processing method can be found in [25].
It can be noted that in comparison with more advanced far-field propagation methods such as based on solving Acoustic Perturbation Equations (APE) [26] or the hyperbolic part of the generalised acoustic analogy equations [25], the standard FW-H method is simpler. However, it requires an appropriate calibration of the acoustic integration surface including the closing discs which should be adjusted a-posteriori by comparison with the far-field noise data. In the present work, the calibration of the FW-H surface is performed for the LES solution of the CoJeN OP1.3 case on the coarse grid (Mesh #2). Having done this, the same acoustic integration surface is applied for all other CoJeN calculations: no additional adjustment of the integration surface was performed to obtain the far-field noise predictions reported in the results section.

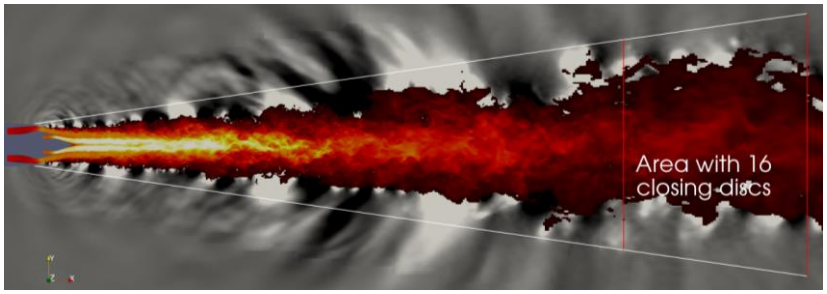


**Figure 3**. Instantaneous velocity magnitude and pressure field for the OP1.3 simulation on Mesh#1 and the location of acoustic surfaces used in the FW-H method

D. GPU Computing

All 6 CoJeN cases are computed on several home-office computer workstations which utilise the current solver capability to perform flow and noise predictions using single-precision floating point accuracy without a notable loss in accuracy. One set of workstations is equipped with 2 "gaming" NVidia GTX1070 (8GB) GPU cards each and connected via MPI communication, while the other single workstation is equipped with 2 (newer generation) Titan RTX (24GB) GPUs. Performance of these GPUs for computing the LES solution of the CoJeN OP1.3 jet case on each grid for 100 convective time units (TUs) is compared in table 2. Although slight case dependent, the 4x GTX 1070 cards achieve 60 TUs per day for Mesh#1, and 100 TUs per day for Mesh#2. The Titan RTX cards are a newer and faster type of GPU cards as well as having a larger memory size in comparison with the GTX1070 cards and are 1.4-1.6 times faster in this case. However, at present the former are less cost-effective as the price of 4x GTX 1070 is less than that of 1x Titan RTX card. It should be noted that 1 convective time unit of the simulation corresponds to the time taken by a turbulent eddy travelling at a speed equal to the jet core velocity to cover the distance equal to 1 bypass nozzle diameter. For comparison, 200 TUs are used as the spin-out time to reach a statistically stationary LES solution and the solution collection time for the subsequent statistical analysis corresponds to a further 400 TUs. In terms of real time units, for the statistical signal this means 0.23 seconds for the fastest jet to 0.50 seconds for the slowest jet simulated.

**Table 2. LES run times for the CoJeN OP1.3 jet case**

| GPU Setup/Mesh Type | Mesh #1 (82 $10^6$ Cells) | Mesh #2 (50 $10^6$ Cells) |
|---|---|---|
| 4x NVidia GTX 1070 (8GB) | 60 TU per day | 100 TU per day |
| 2x NVidia Titan RTX (24 GB) | 100 TU per day | 160 TU per day |

It should be pointed out thanks to the use of the GPU-tailored LES method the current time to solution shows an order of magnitude reduction in comparison with the conventional LES methods (for a detailed discussion of GPU LES versus CPU LES run times, see [12]).

# Results

A. Validation of the meanflow velocity and turbulence solutions

Following the literature [9,10], the CoJeN OP1.3 jet case, which corresponds to the heated jet core stream at the highest velocity, is considered for validation of the LES solutions. Figs.4 and 5 show distributions of the streamwise component of the meanflow velocity, its root-mean-square (r.m.s.) fluctuation, and the turbulent kinetic energy along the jet centreline and for several radial profiles downstream of the central body. The centreline distributions are normalised by the jet velocity at the core nozzle exit. The CABARET solutions on the two grid resolutions, Mesh#1 and Mesh#2 are

compared with the experimental data and with the reference Lattice Boltzmann Method [10]. Notably, the CABARET solutions on the two grids virtually coincide as shown in fig.4 (left and centre) and fig.5. For both the grids, the CABARET solution captures the experimental data well including the initial wake region downstream of the central body, which is most noticeable in fig 4 (centre), for x/Dj<4.0. It should be pointed out that an essential element of accurate modelling of the flow dynamics downstream of the nozzle exit and its interaction with the central body is the use of turbulent inflow conditions at the inlet of each nozzle stream. These conditions have been implemented in the CABARET solutions for the first time in the literature. To illustrate this, figure 4(right) shows the velocity fluctuations for the same OP 1.3 case on Mesh#2, with and without turbulent inflow conditions: in comparison with the initially laminar solution, the CABARET solution with the synthetic turbulence applied at the nozzle inlet shows a closer agreement with the experiment for the first 4 jet diameters downstream of the nozzle exit.

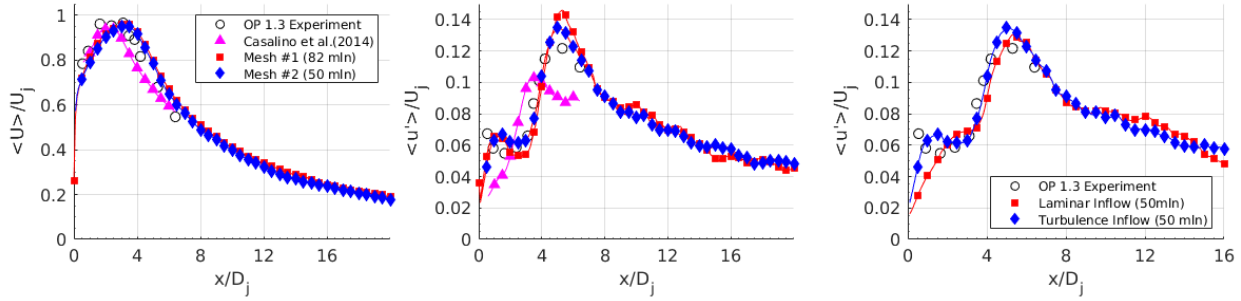


**Figure 4.** Mean axial velocity (right) and mean axial velocity fluctuations (centre) results for OP13 ($U_j$=480.7) from LES compared to experimental values and LBM results taken from [10]. The results on the velocity fluctuations when using the turbulent inflow condition compared to a laminar inflow condition (right).

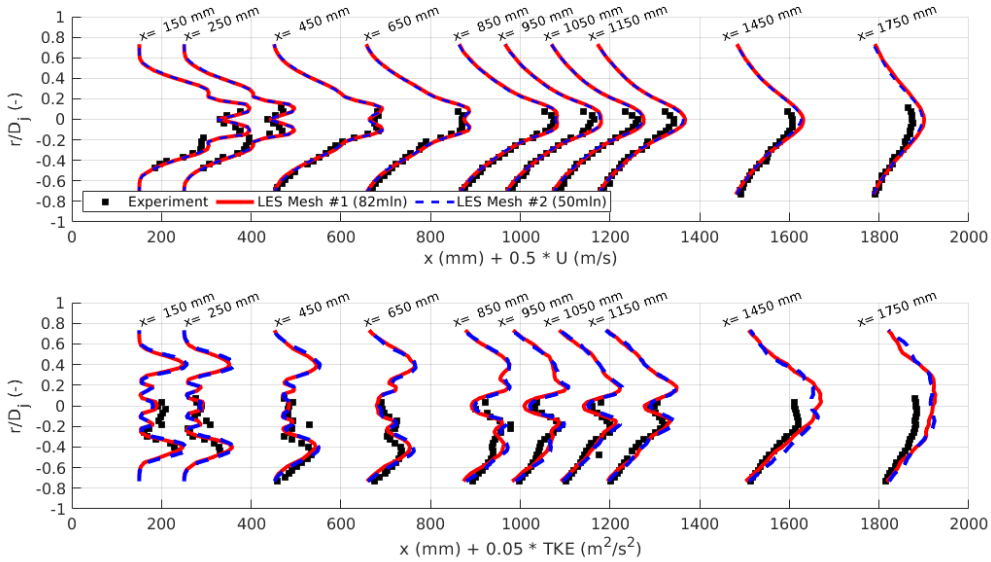


**Figure 5**. Radial profiles of mean velocity and mean turbulent kinetic energy for OP1.3 at several locations along the jet axis. The experimental results (black squares) digitised from [10] are compared to the results obtained on the two grids (Mesh#1 is red and Mesh#2 is blue). In consistence with the literature, in this figure, the stream-wise coordinate x is measured from the outer nozzle lip.

B. Validation of the far-field noise spectra solutions

Using the FW-H surface with a suitably defined set of acoustic integration surfaces, far-field noise spectra predictions are computed for all 6 CoJeN cases. Fig.6 shows results for the noise spectra predictions of the OP1.3 jet, corresponding to the heated jet core at a supersonic acoustic Mach number on the two LES grid resolutions, Mesh#1 and Mesh#2. The noise predictions on both grids are in a good agreement with each other. The spectra predictions also show the expected trend in comparison with the experiment: since the accuracy of predictions improves as the grid becomes finer. For example, the noise spectra predictions on the coarse mesh of 50 $10^6$ cells (Mesh#2) are within 2-3dB error from the experiment for frequencies from $0.02 < St_D < 5\text{-}6$ and a wide range of polar angles 30-90° to the jet flow. Here the

Strouhal number $St_D$ is defined on the jet core stream velocity and the bypass nozzle diameter. In comparison with the coarse grid predictions, the accuracy of noise spectra predictions based on the fine grid of 82 $10^6$ cells (Mesh#1) are improved to become 1-2dB in comparison the experiment for the same range of sound frequencies and microphone angles. Notably, on this grid the peak noise is captured with an error of less than 1dB. It can be further noted that the 2-3dB accuracy of flow and noise predictions on the coarse LES grid which corresponds to faster turn-around solution times is still generally acceptable. The same accuracy is also achieved for the remaining 4 CoJeN cases from table 1 which were run on Mesh#2.

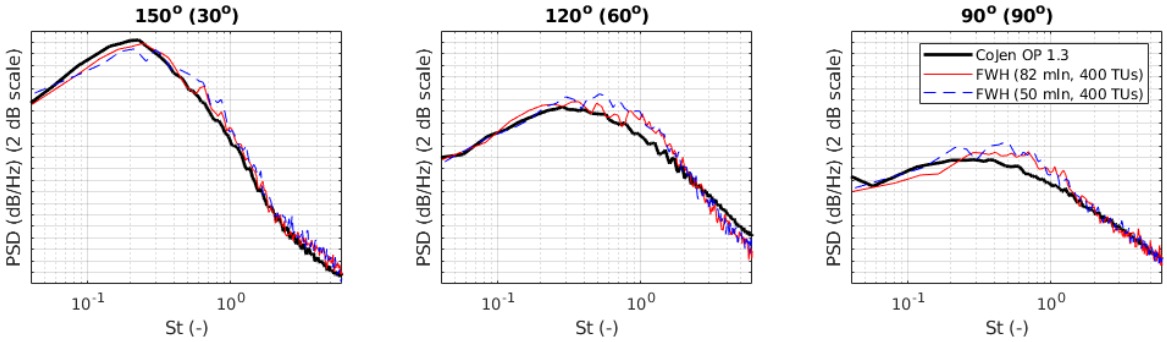


**Figure 6**. Sound predictions at three angles: for OP 1.3 and two different meshes.

Fig. 7 shows the LES predictions of the relative Over All Spectra Level (OASPL) directivity between several pairs of the 6 CoJeN jets (table 1), which differ by the jet Mach number (fig.7, left) and also by the core-stream temperature (fig.7, right) in comparison with the same datasets from the experiment. The OASPL are obtained by integration of the corresponding narrowband spectra from $St_D$ =0.1 to $St_D$ = 3 in each jet case. Notably, the LES based results of the acoustic predictions capture the trends of the experiment with an error of 0.5-1dB for most observer angles and pairs of the jet cases. A detailed discussion of the Mach number and temperature effects on the co-axial jet noise can be found in [27].

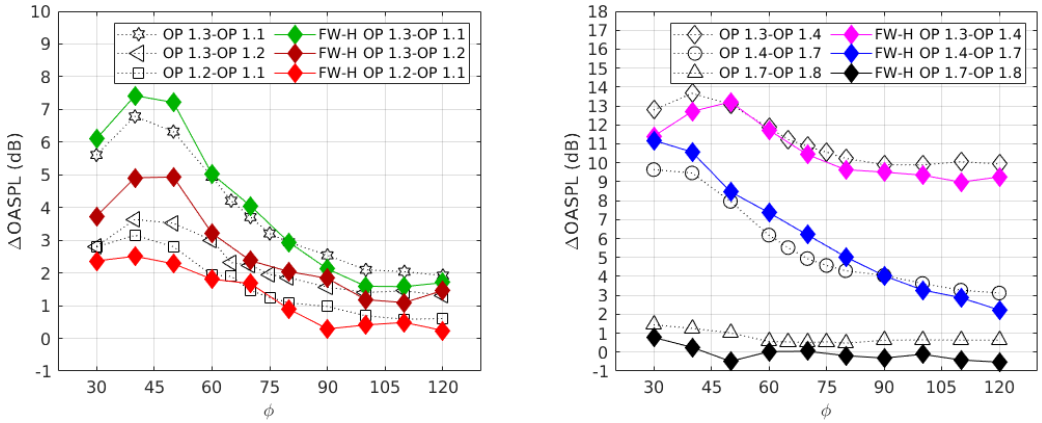


**Figure 7.** Over All Sound Pressure Level (OASPL) comparison with the experiment: comparison of relative dB between different pairs of CoJeN cases.

C. Jet flow structure and its correlation analysis

In the case of the single-stream jet flow (OP1.7), the jet noise is mainly determined by the dynamics of the bypass shear layers which start at the nozzle exit and develop until the collapse of the potential core of the jet leading to the mixed jet flow further downstream (fig. 8, bottom). In comparison with this, the dual stream jet case has an added complexity of the inner shear layer which separates the two jet streams. In addition to different velocities, the streams can also have different temperatures (as in the OP1.3 case). Following the literature [28], the structure of a dual-stream jet flow can be broken down into 3 parts: (i) the initial jet region of non-interacting primary/secondary (core/bypass) and secondary (bypass)/ambient shear layers, (ii) the primary/secondary interaction region , and (iii) the mixed flow region (fig.8, top) whereas the interaction region in the case of a single stream jet (OP1.7) is missing (fig.8, bottom). The radial location of the peak turbulent velocity location in all CoJeN jets is about $r/D_j$=0.38. This corresponds to a smaller effective

aerodynamic radius of the bypass stream in these cases in comparison with the bypass nozzle diameter. The second peak of the turbulent kinetic energy in the dual-stream jet case approximately corresponds to $r/D_j$=0.18.

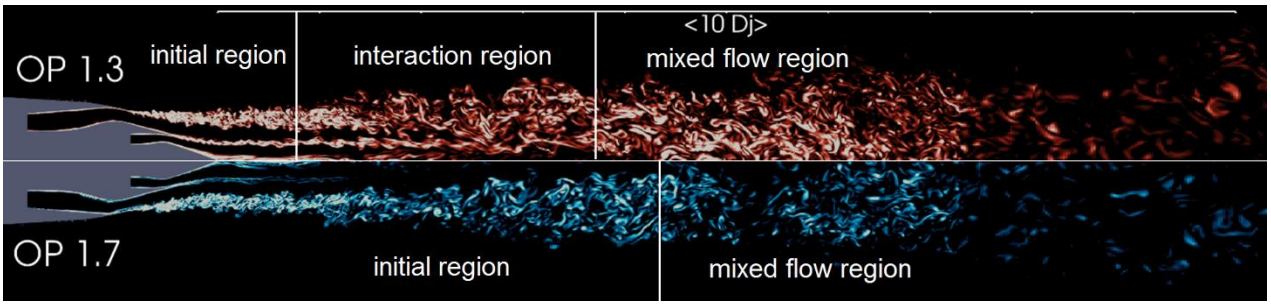


**Figure 8.** Dual-stream and a single stream jet anatomy: contours of vorticity magnitude showing the effect of the inner shear layers in the dual-stream OP1.3 jet in comparison with the single-stream OP1.7 whose core nozzle only generates a rudimentary wake.

In comparison with the meanflow velocity or turbulent velocity fluctuations, which are important for jet aerodynamic properties such and thrust and mixing, it is higher statistical moments of the turbulent velocity fluctuation that determine the properties of noise generated by turbulence in high-speed jet flows. In the framework of acoustic analogy, following the pioneering work of Lighthill [1], many formulations for jet mixing noise modelling are based on re-arranging the original Navier-Stokes equations into some linear sound propagation operator and non-linear source terms, most notably including the work of Lilley [29] and the generalised acoustic analogy by Goldstein [22].

Many acoustic analogy formulations consider the covariance of nonlinear stresses of the momentum Navier-Stokes equations as an effective jet noise source that can be convoluted with an appropriate transfer (Green's) function to calculate noise at the far field. Most consistently, the effective noise source is introduced in the Goldstein generalised acoustic analogy, where the meanflow effect is completely removed from the turbulent fluctuating Reynolds stresses, whose covariance:

$$R_{ijkl}(\mathbf{y};\boldsymbol{\eta},\tau) = \frac{1}{T}\int_0^T \left[v_i'v_j' - \overline{v_i'v_j'}\right](\mathbf{y}-\boldsymbol{\eta}/2,t)\left[v_k'v_l' - \overline{v_k'v_l'}\right](\mathbf{y}+\boldsymbol{\eta}/2,t+\tau)\mathrm{d}t, \quad (1)$$

or, in case the density fluctuations are equally important:

$$R_{ijkl}(\mathbf{y};\boldsymbol{\eta},\tau) = \frac{1}{T}\int_0^T \left[\rho v_i'v_j' - \overline{\rho v_i'v_j'}\right](\mathbf{y}-\boldsymbol{\eta}/2,t)\left[\rho v_k'v_l' - \overline{\rho v_k'v_l'}\right](\mathbf{y}+\boldsymbol{\eta}/2,t+\tau)\mathrm{d}\tau. \quad (2)$$

determines the effective sound sources in the jet.

Here subscripts i,j,k,l=1,2,3 are cylindrical-polar coordinate components (1 is in the jet flow direction, 2 is radial, and 3 is azimuthal), bar corresponds to the simple time or Favre averaging, $\mathbf{y}$ is a coordinate vector corresponding to the effective noise sources in the jet, $\boldsymbol{\eta}$ and $\tau$ correspond to the spatial separation vector and the temporal separation, and $\rho$ and $v_i'$ are the density and flow velocity fluctuations, respectively.

For the dual-stream CoJeN cases considered in the present publication, the $R_{ijkl}(\mathbf{y};\boldsymbol{\eta},\tau)$ is computed for the jet locations corresponding to the inner and the outer aerodynamic radii (as defined in fig.8) where the velocity fluctuations reach the local maxima. In case of the single-stream OP1.7, only the bypass/ambient aerodynamic radius is considered. Spatial separation is defined in the stream-wise direction, $\boldsymbol{\eta} = (\eta_1, 0,0)$, which corresponds to the largest correlation scale of the effective jet noise source stretched by the jet flow direction. Following the literature [30,31,32], several non-negligible correlation function components $R_{ijkl}$ are considered. It is expected that the space-time correlation functions $R_{ijkl}$ mainly depend on the time separation in the laboratory (nozzle) frame, $\tau$, and the space separation in the convective reference frame, $\eta_1 - \tau U_c$, which corresponds to an eddy-convection velocity $U_c$. The physical meaning of the convection velocity is the effective velocity of the noise-radiating part of the coherent structures in the jet flow[33]. The convection velocity is evaluated from the analysis of the LES data. The stream-wise $R_{1111}$ component, which corresponds to the peak sound directivity, is considered in fig 9. Here the process of computation of $U_c$ is shown: fig.9 (top left and middle) demonstrates the correlation fields for the core and bypass aerodynamic radii of the OP1.3 jet whereas fig.9 (top right) shows the same for the bypass radius for the OP1.7 jet. In the figures, the computed convection velocity is compared with the jet velocity at the relevant (core or bypass) nozzle exit, $U_j$ and also with the local meanflow velocity in the stream-wise direction, $U_x$.

For each dataset shown in the figure, the jet location corresponds to the end of the potential core and the correlations are averaged over several azimuthal angles of the axi-symmetric jet to improve the statistical ensemble averaging in each case. Following this procedure, $U_c$ is evaluated as the best fit parameter that leads to the maximum correlation at $\eta_1 =$

$\tau U_c$ for most time separations. Similar to a single steam jet flow, the convection velocity in the outer shear layers of the CoJeN jets is close to the local meanflow velocity and is smaller than the meanflow velocity inside the jet. Having computed the convection speed, the corresponding correlation space and time scales are calculated by setting $\eta_1 = \tau U_c$ and $\tau = 0$ one at a time. Consistent with the jet noise literature [30], the separate space and time correlation functions of the CoJeN jets appear to be well described by an exponential function with a cusp point at zero separation (see fig.9, bottom) and the corresponding dimensionless differential correlation scales are readily computed by fitting the corresponding exponent in each case. Here the correlation space and time scales are normalised by the jet diameter and by the jet diameter and the relevant jet velocity at the nozzle exit, respectively.
It can be noted that the correlation length scale corresponding to the time separation, $L_\tau$, which is measured in the laboratory frame, where the acoustic analogy noise sources are defined, is about 0.1-0.3 time the bypass nozzle diameter. This range of values is in agreement with the acoustic wavelength at peak noise radiation ($St_D$~0.2). It can be further noted that the time scale in the outer shear layer of the OP1.3 jet is more than 2 times smaller in comparison with acoustic length scale of the core/bypass shear layer. The latter suggests that the inner shear layer of co-axial jets is mostly responsible for to low frequency sound radiation. Furthermore, the correlation scale associated with the convective reference frame, $L_\eta$ is 3-7 times smaller and may be attributed to high-frequency noise generated by fine-scale turbulent eddies as they are convected by the flow. To support the latter observation, it can be noted that the small correlation space length scale is more universal compared to the large scales: it is approximately constant across the jet flow.

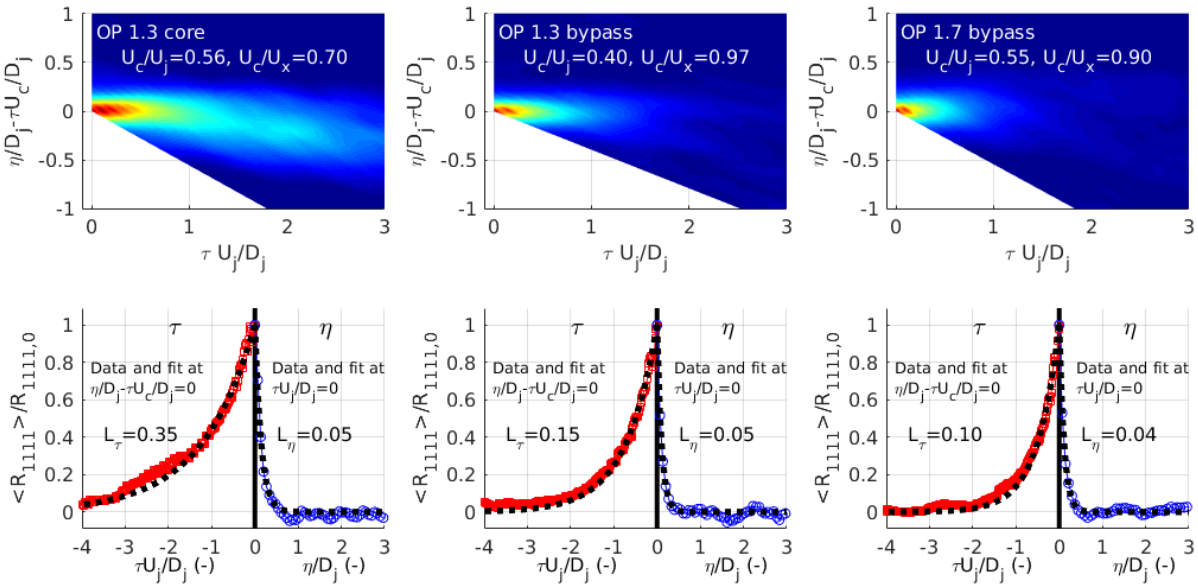


**Figure 9**. Correlation $R_{1111}$ evaluated at the end of the potential core location and the corresponding length and time scale fit for datasets of OP1.3 and OP1.7

D. Similarity scaling of jet flows and their acoustic scales and amplitudes

Jets with different flow conditions do not have the same flow features such as meanflow velocity or fluctuations at the same absolute location from the nozzle exit even when normalised by the perfectly expanded jet velocity and jet diameter. One of the main drivers in the flow physics is the length of the potential core, followed by the jet spread. When these factors are used to normalise the axial and radial coordinates many of the flow statistics are very similar for all flow conditions [34]. In this work, following [35], the two-parameter functional form is used to collapse the centreline velocity distribution of CoJeN jet flows:

$$\frac{U}{U_j} = 1 - \exp\left\{\frac{2\alpha}{1-\frac{x}{\beta D}}\right\}, \quad (3)$$

where α and β stand for case-dependent dimensionless parameters for jet spread and potential core length.

Because of the wake of the central body, the fit needs to be adapted. The decay rate of the centreline velocity is fitted to the similitude form (3) downstream of the end of the jet potential core, which corresponds to the centreline points x/Dj>7-8. The original centreline meanflow velocity profiles of CoJeN jet flows (table 1) exhibit a notable variation depending on the jet core velocity and temperature (fig.10, left). However, once the similitude shape parameters are obtained for

each jet, their centreline meanflow velocity profiles collapse as a function of the dimensionless coordinate $\left(\frac{x}{D}-\beta\right)/(\alpha\beta)$ (fig.10, right).

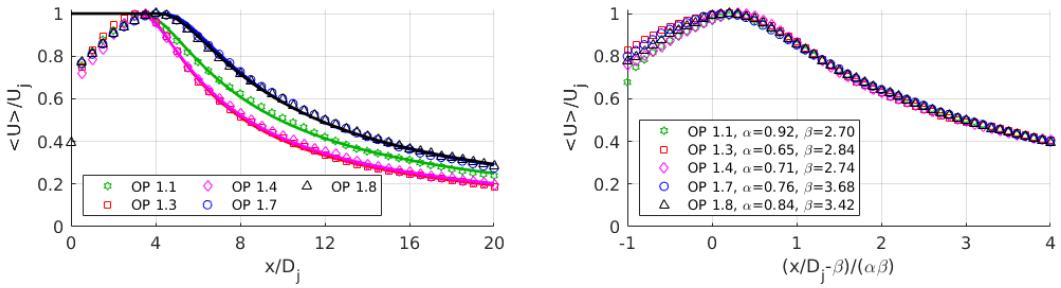


**Figure 10.** Using a two-parameter similitude fit function to collapse the meanflow data of the CoJeN jets

In comparison with the centreline profiles, the turbulence properties in the dual-stream jets exhibit more variation. For example, fig.11(left) shows that there is a sudden change in the convection velocity along the inner aerodynamic radius of the OP1.3 CoJeN jet flow corresponding to the shear layer between the core and the bypass stream. The change of the convection velocity inside the dual-stream jet, which marks the onset of the interaction zone, where the inner and the outer shear layers merge, is particularly striking in comparison with the smooth behaviour of the local meanflow velocity of the jet. The difference in the behaviours also means that the local meanflow velocity in the inner shear layer cannot be used as a relevant variable for scaling of the convection velocity in the inner shear layer of dual-stream jets. In comparison with this, the convection velocity along the outer aerodynamic radius almost perfectly coincides with the meanflow velocity there. The data of the heated and the cold CoJeN jet flows in the bypass/core share layers appear to collapse to two distinct families corresponding to two ratios of the convection velocity to the jet core velocity: $U_c/U_j$~0.6 for the cold jets and $U_c/U_j$~0.4 for the heated jets. The near perfect collapse of the convection and the local meanflow velocity, which happens for all jets except for the low-speed CoJeN case (OP1.1), suggests that the acoustic behaviour of the dual-stream jet flows along the outer aerodynamic radius is very much similar to that of single-stream jets [36].
The above analysis of the LES results is in agreement with empirical co-axial jet models in the literature such as the Institute of Sound and Vibration Research (ISVR) 4-source model [28], which considers the interaction of the inner and outer shear layers a distinct feature of dual-stream jet flows. In accordance with the model, co-axial jets exhibit a behaviour similar to single-stream jets outside of the interaction region. Furthermore, it should be pointed out that the current simulation results, which show collapse or dissimilarity of the jet local velocity and convection velocity depending on the radial jet location, are consistent with the recent experimental observations in multi-stream jets [37].

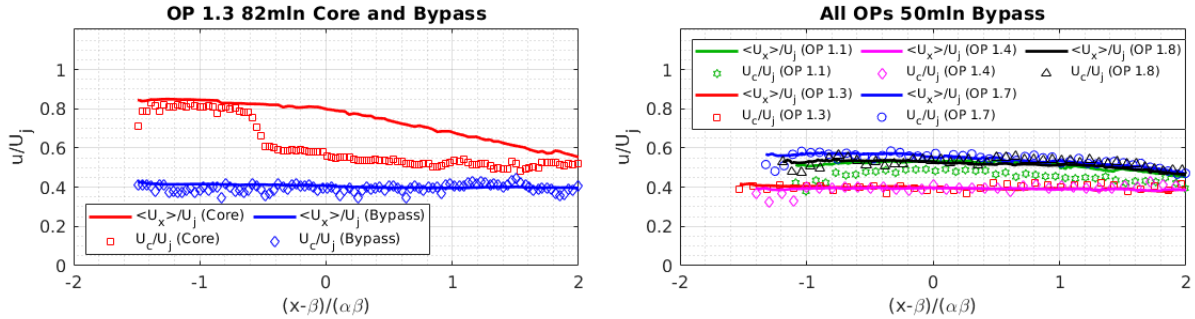


**Figure 11.** The convection speed along the liplines used in the correlation analysis for the core (left) and bypass of the OP 1.3 jet case, and for only the bypass (right) aerodynamic radius for all the other cases.

Fig.12 compares the distribution of the correlation space, $L_\eta$, where $\boldsymbol{\eta} = (\eta_1, 0,0)$ and time scales, $L_\tau$, of the dual-stream OP1.3 jet along the outer aerodynamic radius. For the time scale, both the core length and the decay rate parameters, β and α are used in the non-dimensionalisation. Additionally, the time scale is normalised by the local convection velocity, $U_c$. Furthermore, the same jet velocity at the nozzle exit, $U_j$ is used, consistent with the normalisation of the time scale shown in fig.9, bottom. Both the space and the time scales shown correspond to the stream-wise correlation component, $R_{1111}$. Following the non-dimensionalisation, the length scales are reasonably well approximated by a linear fit function $a + b\bar{x}$, where $\bar{x} = \left(\frac{x}{D_j}-\beta\right)/(\alpha\beta)$ for a range of acoustically important locations along the outer aerodynamic radius. The goodness of a linear approximation suggests that the acoustic length scale of the jet flow grows linearly following the outer shear layer development.

For the space length scale (fig.12, left), the fit parameters, $a$ and $b$ are more or less independent of the LES grid resolution within the linear fit accuracy. Furthermore, the obtained linear fit parameters also are in excellent agreement with the dimensionless length parameters, which are extracted from the PIV data corresponding to the cold single-stream jet flows at SP (Set Point) 3 and 7 operational conditions from the NASA SHJAR database [5]. For example, it can be noted that the linear fit parameters extracted from the LES solution on Mesh#2 virtually coincide with the parameters of the single-stream NASA jets. For the time scale (fig.12, right), the LES results on the two grid resolutions show some more scatter but are still reasonably well approximated by a linear fit. The parameters of the time-scale fit for the OP1.3 jet case fall below the dimensionless scales of the reference set of singles-stream NASA jets although the difference between the two sets of data is not dramatic.
As the next step, dimensionless correlation space and time scales corresponding of several CoJeN jet cases from table 1 are compared with each other and with the dimensionless fit data of the single-stream NASA jets corresponding to SP3 and SP7 conditions (fig.13). The same normalisation based on $\left(\frac{x}{D_j}-\beta\right)/(\alpha\beta)$ is used. In can be noted that the acoustic scales of all the CoJeN jets considered are reasonably well approximated by a linear fit function which has a similar positive slope parameter, $b$ in all cases. The free constant of the linear function, $a$ shows more variation between the different jet cases. Partly, this variation could be associated with the accuracy of obtaining the similitude shape parameters, β and α in each CoJeN jet case.

In comparison with the single-stream-jet-like behaviour of the outer shear layers, the evolution of the acoustic scales inside the dual-stream jet is much more complex. This is illustrated in fig.14 which compares the distribution of dimensionless correlation space and time scale along the outer and the inner aerodynamic radius of the OP1.3 jet case. It should be noted that the same non-dimensionalisation is used here based on the local flow parameters as for the outer shear layer results presented in fig.12. For example, for the normalisation of the time scale in the inner shear layer, similar to the outer shear layer, the local convection velocity is used together with the jet velocity at the nozzle exit. It can be further noted that either the normalisation based on the local convection velocity or the jet meanflow velocity does not help collapsing the data in this case.

In contrast with the outer shear layers, the development of the space and time correlation length scale in the core/bypass shear layer is not monotonic. The non-monotonicity reflects the transition from the initial jet region to the onset of the interaction region at $\frac{x}{D_j}-\beta\approx-0.4\alpha\beta$ and the transition from the interaction region to the mixed flow region at $\frac{x}{D_j}=\beta$. At each of these three jet regions, the evolution of acoustic scales can still be approximated by a linear fit function, but parameters of the fit function are quite different depending on the region, which reflects the growth or decay of the acoustic length scale, as relevant for the dual-stream jet flow physics.

Getting back to the discussion on the jet similarity along the outer aerodynamic radii, fig.15 compares the distribution of relative amplitudes of several major correlation components, $R_{ijkl}(\boldsymbol{y};\boldsymbol{\eta}=0,\tau=0)$ for all 6 CoJeN cases from table 1. The non-dimensionalisation is performed based on the mean turbulent kinetic energy (TKE) in fig.15 (top left) and using the largest correlation amplitude corresponding to the stream-wise propagation direction, $R_{1111}$ $(\boldsymbol{y};\boldsymbol{\eta}=0,\tau=0)$ in the rest of fig 15. It can be noted that the ratio of $R_{1111}$ to the turbulent kinetic energy squared ( $TKE=(\langle v_1'\rangle^2+\langle v_2'\rangle^2+\langle v_3'\rangle^2)/2$) inside the jet approximately stays constant within the range of 1.1-1.4 for all the jet flows. This range of values is in agreement with the usual assumptions about the relative amplitudes of turbulent velocity fluctuations in high-speed axi-symmetric jet flows $\langle v_1'\rangle\approx1.5\langle v_2'\rangle\approx1.5\langle v_3'\rangle$ that leads to the estimate of $\frac{R_{1111}}{TKE^2}\approx1.12$.
Furthermore, for all CoJeN cases considered, the non-negligible relative source amplitudes normalised by the $R_{1111}$ component collapse to 6 distinct families corresponding to different noise directivities: $R_{2222}$ , $R_{3333}$, $R_{1212}$, $R_{1133}$, $R_{1313}$, and $R_{1122}$. The relative values show a small variation around the mean values from case to case and with the position along the outer aerodynamic radius. For future reference, the mean values are summarised in table 3:

**Table 3. Mean values of the relative correlation amplitudes**

| $R_{2222}/R_{1111}$ | $R_{3333}/R_{1111}$ | $R_{1212}/R_{1111}$ | $R_{1313}/R_{1111}$ | $R_{2323}/R_{1111}$ | $R_{1122}/R_{1111}$ |
|---|---|---|---|---|---|
| 0.3 | 0.5 | 0.3 | 0.35 | 0.2 | 0.1 |

Interestingly, the relative source amplitudes shown in the table are the same dominant source components that were considered in the previous models of cold single-stream jets based on the Goldstein generalised acoustic analogy [31]. Again, this reconfirms that in the bypass/ambient shear layer the acoustic source properties of the dual-stream jets are similar to single-stream jets. One notable difference in comparison with the existing single-stream jet models, however, is

that the relative source strengths of diagonal terms, $R_{2222}$ , $R_{3333}$ of the CoJeN jet flows appear to be amplified by a factor 2-3.

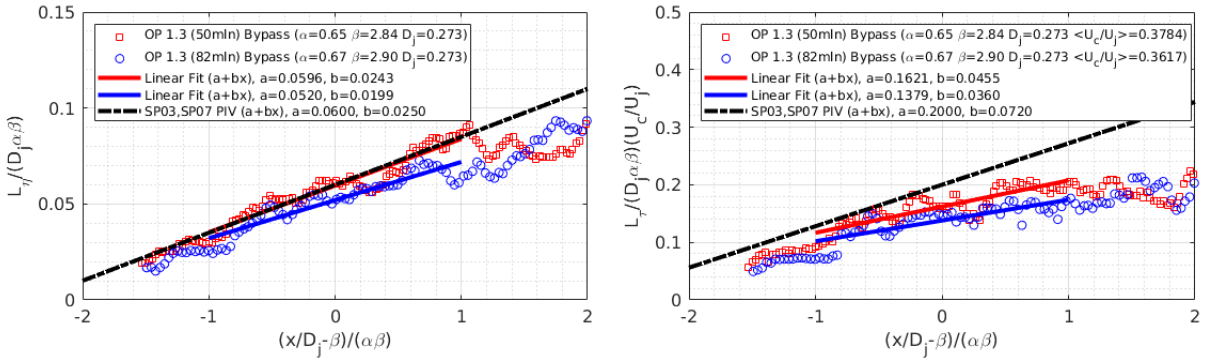


**Figure 12.** The normalised space (left) and time (right) scales extracted from the correlations ($R_{1111}$) for the bypass aerodynamic radius obtained from the 50mln mesh and the 82mln mesh for OP 1.3

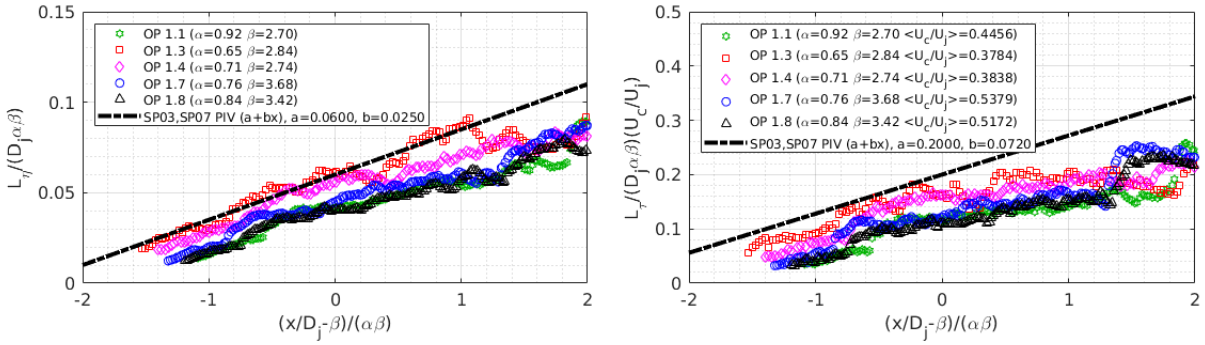


**Figure 13.** The normalised space (left) and time (right) scales extracted from the correlations ($R_{1111}$) for the bypass aerodynamic radius obtained from the 50mln mesh for all operating points considered

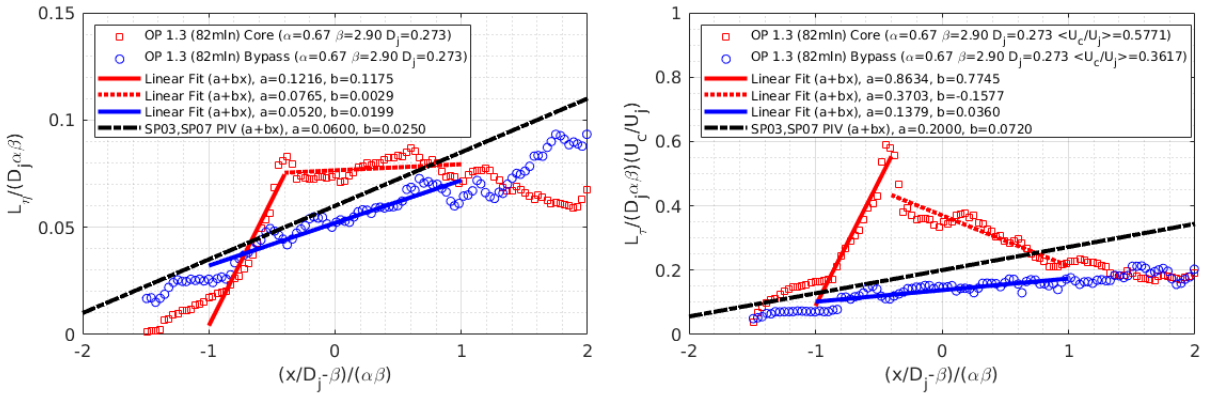


**Figure 14.** The normalised space (left) and time (right) scales extracted from the correlations ($R_{1111}$) for both the core and bypass aerodynamic radius both obtained from the 82mln mesh for OP 1.3

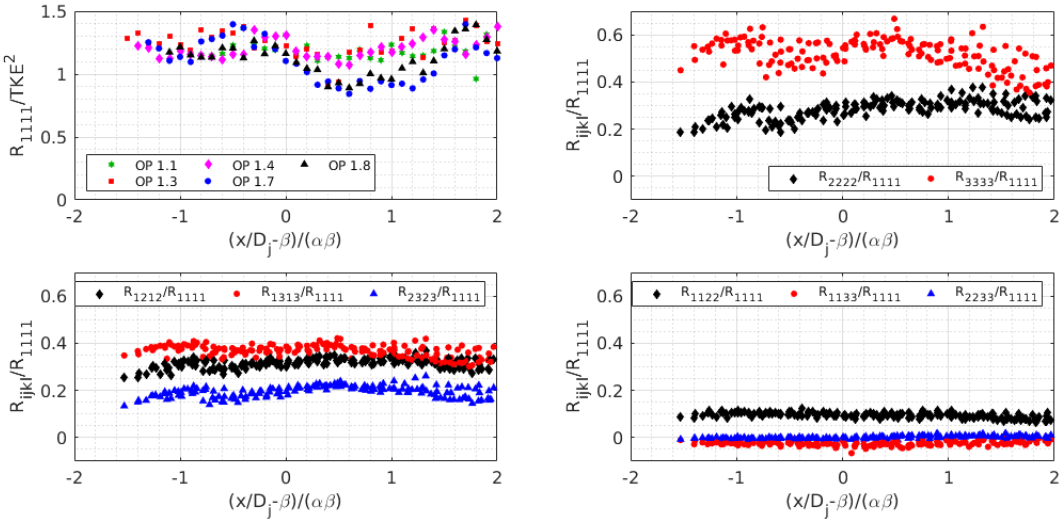


**Figure 15.** $R_{1111}$ component normalised by the turbulent kinetic energy (top-left) and different $R_{ijkl}$ components normalised by $R_{1111}$ of the same case. All CoJen OP data correspond to the aerodynamic radius in each case

# Conclusion

High-fidelity Large Eddy Simulations (LES) are conducted for a representative set of co-axial jet cases corresponding to the CoJeN experiment. The operational parameters of the 6 jet flows considered cover a wide range acoustic Mach numbers and temperatures of the core stream as well as bypass to core stream velocity ratios. In all simulations, the high-resolution CABARET method is applied for solving the Navier-Stokes equations on unstructured meshes based on the OpenFOAM SnappyHexMesh utility. To correctly simulate the turbulent flow downstream of the nozzle exit, a Wall Modelled LES approach is used together with an open-source synthetic turbulence generator to prescribe appropriate turbulent inflow boundary conditions. It is demonstrated that the combined approach works well for accurately capturing of turbulent velocity fluctuations in the wake downstream of the central body of the nozzle. Similar to the previous CABARET simulations based on the Monotonically Integrated LES framework [12] the present approach is implemented on Graphics Processing Units (GPUs). The implementation makes it feasible to run LES on grids 50 and 82 $10^6$ cells in the "compute under desk" mode utilising only a few GPU cards. The flow and noise predictions obtained with the GPU-CABARET method combined with the Ffowcs Williams – Hawkings method are in excellent agreement with the available experimental data. In particular, the noise spectra predictions based on the 82 $10^6$ cell LES grid are within 1-2 dB from the experiment for a good range of polar angles, 30-90$^o$ and Strouhal numbers up to 5-6 while the peak noise is captured with an error of less than 1dB. It also shown that the LES predictions of the relative Over All Sound Pressure Levels (OASPL) for different jet Mach numbers and core-stream temperatures capture the trends of the experiment with an error of 0.5-1dB for most observer angles and pairs of the CoJeN jet cases.

To analyse the structure of effective noise sources of the CoJeN jets in the context of generalised acoustic analogy, the covariance of turbulent fluctuating Reynolds stresses is computed and its space and time correlation length scales are evaluated. For jet locations corresponding to the inner aerodynamic radius, the time scale, which can be associated with hydrodynamic sound sources defined in the nozzle reference frame, is order of the acoustic wavelength of peak jet noise at low frequencies. In comparison with this, the same lengths scale in the bypass/ambient shear layer is more than twice smaller and corresponds to higher frequencies. It is also shown that the small space length scale associated with fine-scale turbulence in the convective reference frame does not depend on the location in the transverse plane to the jet flow. Furthermore, consistent with previous experimental observations in multi-stream jets, the convection velocity in the outer jet shear layers is close to the local meanflow velocity.

An attempt is made to non-dimensionalise the meanflow, the turbulent kinetic energy, and the covariance of turbulent fluctuating Reynolds stresses of different co-axial CoJeN jet flows in order to reveal hidden similarities of their acoustic sources. The non-dimensionalisation is based on the well-known self-similarity property of single-stream axi-symmetric jet flows, where the main drivers in flow physics is the length of the potential core, followed by the jet spread. It is demonstrated that the acoustic properties of different CoJeN jets at the outer aerodynamic radius can be described by the analogy with single-stream jets. In these regions, the distribution of dimensionless acoustic time and space length scales can be reasonably well collapsed to a linear fit function, which parameters weakly depend on the jet case and are not too dissimilar from the dimensionless scales of the single-stream SP3 and SP7 jet flows from the NASA SHJAR database. Moreover, the relative amplitudes of all non-negligible components of the acoustic sources at the outer aerodynamic

radius location of all CoJeN jets considered are approximately constant and converge to the same main sets of values corresponding to 7 major correlation components $R_{1111}$, $R_{2222}$ , $R_{3333}$, $R_{1212}$, $R_{1133}$, $R_{1313}$, and $R_{1122}$ when non-dimensionalised by the turbulent kinetic energy. These components are approximately the same ones as were used in the previous single-stream jet noise models based on acoustic analogy. In comparison with the linear behaviour of the acoustic scales in the outer shear layers, the variation of acoustic properties in the jet locations corresponding to the inner aerodynamic radius of dual-stream jets is much more complex. For these locations, the evolution of the correlation space and time scale is non-monotonic and strongly depends on the specific jet region – initial, interaction or mixed flow. An optimal choice of the scaling parameters that would allow one to collapse acoustic characteristics of different jet datasets in the inner layer remains an open question.

From the perspective of reduced-order modelling of co-axial jet noise, the current research reveals that the acoustic sources in the interior shear layer should be treated differently in comparison with those in the outer shear layer. The analysis provides foundation for empirical low-order approaches, such as the ISVR 4-source model, where the co-axial jet flow is decomposed into separate flow regions corresponding to the initial, interaction, and mixed-flow zones, where different approximations about the jet flow physics are made. The presented analysis is also a useful reference point for future hybrid RANS-LES models [31,38] of co-axial jet noise including low-order models [39] which could be relevant for parametric studies aimed at jet noise reduction in the context of Multidisciplinary Design Optimisation.

# Additional Information

**Acknowledgments**

The CoJeN data used in the current study have been produced by QinetiQ. The authors are grateful to Craig Mead for making the CoJeN noise data readily available and to Dr James Bridges for sharing the PIV data of single-stream NASA SHJAR jets. Fruitful discussions with Dr Vasily Semiletov are gratefully acknowledged.

**Funding Statement**

The research has been supported by the Aero Acoustic Research Consortium, which is administered by Ohio Aerospace Institute and also by the Engineering and Physical Sciences Research Council (EP/S002065/1).

# References

1. Lighthill, M.J. 1952. On Sound Generated Aerodynamically. I. General Theory. *Phil. Trans. Royal Soc. A.* **211**, 564-587.
2. Tanna, H.K. 1977. An experimental study of jet noise: Part I turbulent mixing noise," *J. Sound Vib*., 50, 405–428.
3. Shur, M. L., Spalart, P. R., Strelets, M. Kh. 2005 Noise Prediction for increasingly complex jets. Part I: Methods and tests. Part II: Applications. *Int. J. Aeroacoustics*, 4(34), 21366.
4. Bodony, D. and Lele, S. K. 2008. Current status of jet noise predictions using large-eddy simulation. *AIAA J*., 46:364–380.
5. Bridges, J. and Wernet, M.P. 2011. The NASA Subsonic Jet Particle Image Velocimetry (PIV) Dataset, *NASA/TM*-2011-216807.
6. Skeen, A. 2006 The development of high-speed PIV techniques and their application to jet noise measurement. *PhD thesis*, University of Warwick
7. Tinney, C. E. and Jordan, P. 2008 The near pressure field of co-axial subsonic jets. *J. Fluid Mech*. 611, 175–204, DOI: 10.1017/S0022112008001833.
8. Mead, C.J., Wrighton, C., Britchford, K. 2015. An Experimental Study of Co-Axial Jets Using Acoustic, PIV&LDA Methods (CoJen), *AIAA* 2015-3122.
9. Vuillot, F., Lupoglazoff, N., Rahier, G. 2008. Double-stream nozzles flow and noise computations and comparisons to experiments, *46th AIAA Aerospace Sciences Meeting and Exhibit*. 7 - 10 January 2008, Reno, Nevada.
10. Casalino, D. and Lele, S.K. 2014. Lattice-Boltzmann simulation of coaxial jet noise generation, CTR, Proc. the Summer Program.
11. Housman, J.A., Stich, G.-D., Kiris, C.C., Bridges, J. Jet Noise Prediction using Hybrid RANS/LES with Structured Overset Grids. 2017. *23rd AIAA/CEAS Aeroacoustics Conference*, AIAA 2017-3213.
12. Markesteijn AP and Karabasov SA. 2018. CABARET solutions on graphics processing units for NASA jets: Grid sensitivity and unsteady inflow condition effect. *Comptes Rendus – Mecanique*, 346 (10), 948-963.
13. Iserles, A., 1986. Generalized Leapfrog methods. *IMA J. Numer. Anal*. 1986; 6. 381–392.
14. Roe, P.L. 1998. Linear bicharacteristic schemes without dissipation. *SIAM J. Sci. Comput*. 19: 1405–1427.
15. Goloviznin, V.M., Samarskii, A.A., 1998. Difference approximation of convective transport with spatial splitting of time derivative. *Math. Model.* 10:86–100.

16. Karabasov, S.A., and Goloviznin, V. M. 2009. Compact accurately boundary-adjusting high-resolution technique for fluid dynamics. *J. Comput. Phys.* 228.19: 7426-7451.
17. Semiletov, V. A., and Karabasov, S. A. 2013 CABARET scheme with conservation-flux asynchronous time-stepping for nonlinear aeroacoustics problems", *J. Comp. Physics*, 253(15), 157165.
18. Faranosov, G. A., Goloviznin, V. M., Karabasov, S. A., Kondakov, V. G., Kopiev, V. F., Zaitsev, M. A. 2013. CABARET method on unstructured hexahedral grids for jet noise computation. *Comp. and Fluids*, 88, 165-179.
19. Park, G. I. and Moin, P. 2016. Numerical aspects and implementation of a two-layer zonal wall model for LES of compressible turbulent flows on unstructured meshes. *J. Comput. Phys*. 305, 589-603.
20. Mukha, T., Rezaeiravesh, S. and Liefvendahl, M. 2018. A Library for Wall-Modelled Large-Eddy Simulation Based on OpenFOAM Technology.
21. Saad, T. Cline, D., Stoll, R. and Sutherland, J.C. 2014. Scalable Tools for Generating Synthetic Isotropic Turbulence with Arbitrary Spectra. http://dx.doi.org/10.2514/1.J055230.
22. Richards, A. Saad, T. and Sutherland, J.C. 2018. A Fast Turbulence Generator using Graphics Processing Units, AIAA AVIATION Forum, (AIAA 2018-3559). https://doi.org/10.2514/6.2018-3559Goldstein, M.E. 2003. A generalized acoustic analogy. *J. Fluid Mech.*, 488, 315-333.
23. Goloviznin, V.M., Zaitsev, M.A., Karabasov, S.A., and Korotkin, I.A. 2013. New CFD Algorithms for Multiprocessor Computer Systems (in Russian), Mosk. Gos. Univ, Moscow, ISBN: 978-5-211-06426-3
24. Karabasov, S.A., Bogey, C., and Hynes, T.P. 2013. An investigation of the mechanisms of sound generation in initially laminar, subsonic jets using the Goldstein acoustic analogy, *J. Fluid Mech.* Vol. 714, 24 – 57.
25. Semiletov VA and Karabasov SA. 2018. A volume integral implementation of the Goldstein generalised acoustic analogy for unsteady flow simulations. *J. Fluid Mech*. 853, 461-487.
26. Ewert, R. and Schröder, W. 2003. Acoustic perturbation equations based on flow decomposition via source filtering. *J. Comp. Phys.* 188 (2), 365-398.
27. Markesteijn, A.P. and Karabasov, S.A. 2019. An LES Study of Core Temperature, Velocity, and Mach Number Effect on the Far-Field Noise of Co-Axial Jets, 25th AIAA/CEAS Aeroacoustics Conference (Aeroacoustics 2019), 20 - 23 May 2019, Delft, The Netherlands, *AIAA Paper* 2019-2536.
28. Bryce, W.D. and Chinoy, C.B. 2016. A method for predicting static-to-flight effects on coaxial jet noise. *J. Sound Vib*. 375 (2016) 132–161
29. Lilley, G.M. 1958.On the Noise from air jets. *Aeronaut. Res. Council Rep. Mem*. 20, 376.
30. Harper-Bourne M. Jet noise turbulence measurements. 2003. *AIAA-2003-3214*, 9th AIAA/CEAS aeroacoustics conference.
31. Karabasov, S.A., Afsar, M.Z., Hynes, T.P., Dowling, A.P., McMullan, W.A., Pokora, C.D., Page, G.J. and McGuirk, J.J., Jet Noise: Acoustic Analogy informed by Large Eddy Simulation, *AIAA J*., 2010. 48(7), 1312-1325
32. Leib, S. J. and Goldstein, M. E. 2011. Hybrid Source Model for Predicting High-Speed Jet Noise. *AIAA J*, 49(7), 1324–1335
33. Jordan P. and Colonius, T. 2013. Wave Packets and Turbulent Jet Noise. *Ann. Rev.Fluid Mech*. 45. 173-195.
34. Witze, P. O. 1974. Centerline velocity decay of compressible free jets. *AIAA J*., 12(4), 417–418.
35. Bridges, J. 2016. Simple Scaling Of Multi-Stream Jet Plumes For Aeroacoustic Modeling. *AIAA SciTech Conference* –4-8 Jan 2016.
36. Semiletov, V.A., Karabasov S.A. 2017. On the similarity scaling of jet noise sources for low-order jet noise modelling based on the Goldstein generalised acoustic analogy. *Int. J. Aeroacoustics*, 16 (6), 476-490.
37. Bridges, J. E. and Wernet, M. P. 2017. Measurements of Turbulent Convection Speeds in Multistream Jets Using Time-Resolved PIV," 23rd AIAA/CEAS Aeroacoustics Conference, *AIAA Paper* 2017-4041.
38. Depuru Mohan, N.K., Dowling, A.P., Karabasov, S.A., Xia, H., Graham,O., Hynes, T.P. Tucker, P.G. Acoustic sources and far-field noise of chevron and round jets. 2015. *AIAA J.* 53 (9), 2421-2436.
39. Gryazev, V., Markesteijn, A.P. and Karabasov, S.A. 2019. Low-Order Models of Dual-Stream Jet Noise with Temperature Effects Based on the Goldstein Generalised Acoustic Analogy, 25th AIAA/CEAS Aeroacoustics Conference (Aeroacoustics 2019), 20 - 23 May 2019, Delft, The Netherlands, *AIAA Paper* 2019-2665.